Effect of Doping Silver Nano Particle-enhanced Titanium Dioxide with Organic Luminescent Materials for Solar Cell Application

David Kimemia Njoroge[1*], Walter Kamande Njoroge[2], Isaac Waweru Mwangi[3], Mathew Tonui[4]

[1]*Ph.D. Student, Department of Physics, Kenyatta University, Nairobi, Kenya*
[2]*Senior Lecturer, Department of Physics, Kenyatta University, Nairobi, Kenya*
[3]*Senior Lecturer, Department of Chemistry, Kenyatta University, Nairobi, Kenya*
[4]*Lecturer, Department of Chemistry, Kabianga University, Kericho, Kenya*

Abstract: **Energy is as an important resource to support and is mainly driven by fossil fuels which are easily available and convenient to use. However, these highly treasured commodities produce exhaust gases that severely damages our environment ending to global warming. To mitigate the negative effects of the fuels, solar radiation has been exploited to generate electrical clean (green) energy using photovoltaic cells. However, solar radiation is not constant at all times of the day and also varies depending on the season of the year. This study involves the application of organic fluorescent materials to prolong solar cell output. The different luminescent materials were analysed using Fourier Transformed Infrared spectroscopy (FTIR) and then applied in the construction of a photocell. This was done by doping titanium dioxide with silver nano-particles at a ratio of 9:1 then mixed the resultant with a fluorescent material. To different samples of the doped material, varying masses of each respective luminescent material were added to the photoactive material. The mixtures were separately placed in a molding dice and compressed at 10 psi for ten minutes, and to that a known mass (0.16 g) of iodine graphite powder-potassium iodate were introduced over the photoactive layer and compressed at the same pressure to enable them bind sufficiently to form a cell. The resulting cell was then characterized under visible radiation. The cell potentials of allicin, gingerol and flourene doped were found to be 0.486, 0.363, and 0.397 V respectively and the fill factor/efficiency (FF / η) of 0.618 / 4.88 %, 0.294 /5.7 % and 0.217 / 2.81 % in the same order after the radiation was withdrawn. The luminescent materials enabled photo activity to generate electricity even after withdrawal of the natural radiation thus had promising properties for photo voltaic devices application.**

Keywords: **Fluorescent solar cells, organic fluorescent materials, radiation delay, synthesis.**

1. Introduction

The use of organic photo fluorescent materials to extend the duration of radiation can enhance generation of electricity in photovoltaics cells. This improved their performance and coupled by their low-cost may result in their potential future utilization. Despite solar radiation not being constant at all times of the day and also differs depending on the season of the year, the available radiation can be harnessed by the use of photo luminescent material modified for the generation of electricity. The best powders which emit electro-luminescent colours dependent mainly on the applied background lighting for their applications [1]. An example of such is when rhiodamine is exposed to different monochromatic radiations, it fluorescence giving a myriad of colours ranging from greenish to yellow on the frequency of the illuminating radiation [2].

The use of fluorescent materials can therefore alleviate direct dependence of normal solar irradiation (DNI) in solar cell devices. This can be achieved by trapping incident solar radiation, at a certain wavenumber and release emissions at a different wavenumber later. Such a delay can be utilized to extend supply of energy for a predetermined period after the source of solar radiation diminishes [3]. These dopants introduce defect traps and alter the band gaps of the host material [4]. This study envisaged to address the challenges encountered by solar irradiance dependent devices with limited spectral response that limits their expected efficiency at different times and seasons of the year. Doping them with sensitizers lowered their band gap and extended absorption range, with the effect of widening the time scope of radiation supply to the host material due to afterglow, at diminished natural radiation. The research considered use of organic based fluorescent materials from plants and synthetic materials known to contain substantial fluorescence and were observed to support delayed radiation. These were allicin and gingerol of garlic and ginger plant origin as flourene was sourced from chemical manufacturers in its powder form. These materials were investigated for radiation delay application and improved efficiencies after the natural solar radiation diminishes. The absorption wavenumbers were 490 cm⁻¹ emission range 500–600 cm⁻¹ for allicin for fluorene excitation peak at 261 cm⁻¹ with an emission peak at 302 cm⁻¹ and gingerol was wavenumbers of 420 cm⁻¹ emission and excitation wavenumber of *350* cm⁻¹.

The titanium dioxide was doped using silver nano particles generated in-situ by reduction of silver nitrate with hydrazine hydrate [5]. The Silver-doping process increases the photo activity of titanium dioxide to be sensitive within the visible

light region. Then the activated titanium dioxide was further doped with the fluorescent materials and their effect on the absorbed radiation to harness the generated potential (V) by solar cells under minimum irradiance conditions was investigated.

2. Materials and Methods

A. Experimental Design

The study applied experimental processes to analyze the organic photo fluorescent and the doped host materials. The process involved a quantitative research design which was carried out first in laboratory for the initial preparation of all the chemicals and material used in the study. Then the prepared materials were then used to prepare the cells in the workshop. The cells were then exposed to solar radiation in an environment open to the sky to harness solar radiation for ten minutes. Then the excited cells were then quickly transferred to a dark room for I-V and P-t characterization.

Figure 1 shows a schematic presentation of the solar cell fabrication process flow diagram.
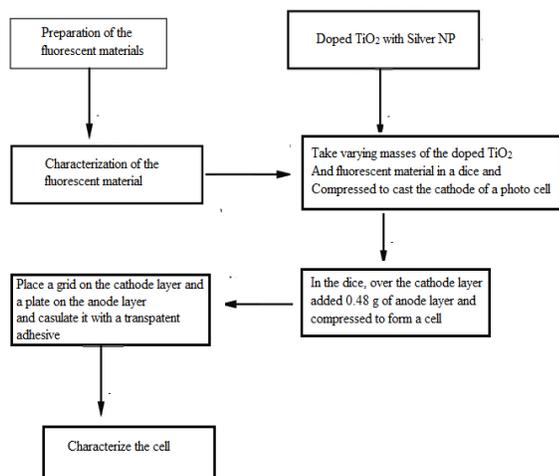
Fig. 1. Flow diagram of the solar cell fabrication process

B. Chemicals and Reagents

The titanium dioxide, flourene, silver nitrate, hydrazine hydrate, graphite, iodine ethanol, acetone and potassium iodide were obtained in their analytical forms from Sigma Aldrich while garlic and ginger were sourced from Wakulla market which is a local market in Nairobi. The organic allicin and gingerol samples were obtained by mixing (2 kg) of chopped (5×5) mm sized pieces of fresh garlic and ginger plant roots respectively and the resulting products separately immersed in a mixer of 100 ml of acetone double deionized water mixture at a ratio of 1:1. Extraction was then carried out using rotary evaporator at 70 ^{0}C. The extract was then dried on a watch glass at (25 °C) room temperature in the open sun and applied in its powder form. Flourene was applied in its powder form as sourced from the chemical manufacturers.

The silver nanoparticles were made through the reduction of silver nitrate with hydrazine hydrate in water ionic liquid micro emulsion. The resultant material was washed thoroughly using water and rinsed with acetone. That Silver-doping increased

titanium dioxide photo activity to be sensitive within the visible light region.

C. Cell Fabrication

The preparation of the cell involved first mixing (10 % Ag ions) with six (5.00 g) constant mass of (TiO_2) photoactive material different samples and separate (0 - 0.06) g varying masses of flourene, allicin and gingerol fluorescent materials. The doped photo active cells were fabricated by taking finely ground 0.09 g (Ag ions enhanced TiO_2 /fluorescent dopant) samples separately in a molding dice, and pressed at constant pressure of 10000 psi. The externally drifted electrons were conducted back to the cell using the graphite-iodine (0.16) g anode layer. Addition of iodine (I_2) restored the excited electrons while potassium iodate (KI) enabled an even dispersal of the species in the (Cx /I/KI) anode complex. The photo anode was prepared by disposing constant 0.3 g, 0.17 g and 0.01 g (Cx /I/KI) mass ratios to the previously formed photo sensitive layer and compressed to form the complete photo active cell. The resulted layers of the fluorescent photo active cells were then carefully removed and placed on a conductor to enable measurement of their I-V and V-T characteristics.

D. Instrumentation

The functional groups in all the fluorescent dopants were confirmed by examining the absorbed infrared radiation of Figure 2.
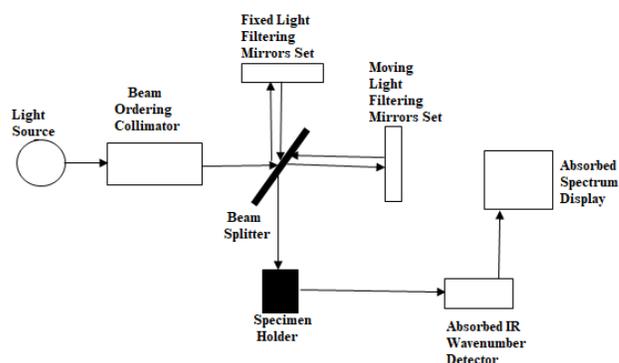
Fig. 2. Schematic presentation of a *Fourier-transform infrared spectroscopy*

The organic materials used in the study were analysed using a Shimadzu FTIR 2014 spectrophotometer whose schematic presentation as shown in Figure 2. The equipment is used in the identification and confirmation of many organic groups is in organic compounds based on the vibrational frequencies of each respective functional group which is unique and characteristic of each respective functional group [6]. The instrument exploits the vibration of molecules where each functional group has its own discrete vibrational energy.

The functional groups in the fluorescent dopants were therefore confirmed by obtaining their respective resonance frequencies [6]. The instrument exploits the vibration of molecules where each functional group has its own discrete vibrational energy. That energy absorbed by the sample is used to identify a molecule as it is particular to each of the respective specific functional group. Therefore, it was used to chemically

characterized the different organic compounds (allicin, gingerol and flourene) used in this study.

The idea behind this infrared analysis began in the 1950's by Wilbur Kaye (1954) which is based on the fact that a molecule consists of two or more atoms with certain distances between them which are determined by sum of all forces between the atoms. When the molecule takes up energy, the atoms are excited to vibrate around their equilibrium state. The vibration energy is quantized, which means it can only have certain values described by quantum numbers. Radiation is emitted during the transition of molecule vibration from the excited state to a lower or the ground state. The frequency principle must be fulfilled, which says that the frequency of the incident light must equal the energy difference between electron orbits (molecule vibrations). The diatomic molecule can be viewed as a one-dimensional harmonic oscillator with the vibrating masses m_1 and m_2 on a weightless elastic spring. The stretching frequency of a bond can then be approximated by Hooke's law which state that the frequency of the vibration v of the spring is related to the mass m and the force constant k of a spring as given in the equation below.

$$v = \frac{1}{2\pi}\sqrt{\frac{k}{m}}$$

Where
v = frequency of vibration
k = elastic force constant
m = mass

E. Cell Characterization

The circuit below was used to obtain the parameters of interest.
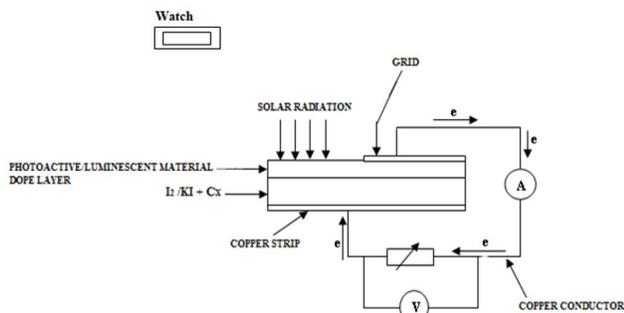
Fig 3. Schematic presentation of the cell characterization circuit

The characterization of the modified solar cells involved the measurement of the generated short-circuit current (I_{SC}), the open-circuit voltage (V_{OC}), after which the fill factor (FF) and the solar energy conversion efficiency (η) were established.

3. Results and Discussion

This section presents the basic active chemical structures functional groups, IR spectrums of the chemically characterized organic dopant materials, {(current (I mA) against potential (V) and (potential(V) against time(minutes)} characterization of the organic materials doped -TiO$_2$ fluorescent solar cells.

A. FTIR Analysis of Allicin in Garlic

The fluorescent material was characterized using a Shimadzu FTIR Prestige-21 spectrometer model 800 series from 4000 to 250 cm^{-1} with scan speed 20 cm^{-1}.The spectrum obtained of allicin was presented in Figure 4.
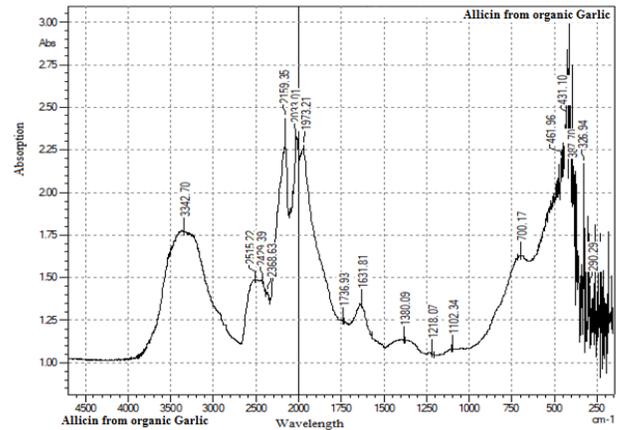
Fig. 4. FTIR spectrum of allicin luminescence material in garlic

The results of Figure 3 confirmed varying resonating moments within the allicin organic luminescent material. The spectrum validated the presence functional groups responsible for fluorescence. The evident divergent (CH$_2$=C), (C=H), (C-O) and (H-NH) functional groups oscillated at $\tilde{V}_{(2515.22, 2429.39\ and\ 2368.63)}$cm^{-1}, $\tilde{V}_{(2159.35, 2033.01\ and\ 1973.21)}$cm^{-1}, $\tilde{V}_{(1102\ to\ 700)}$ cm^{-1} and $\tilde{V}_{(3342.70)}$ cm^{-1} respectively. A similar observation was reported by [7] in their analysis of garlic extracts. The conjugated bonds in combination with alphatic/alicyclics complement each other in fluorescence of the dopant organic materials [8]. The presence of σ- π double bonds enable absorption of radiation due to their constant vibration and rotation of their molecules [9].

B. Response of Allicin Doped TiO$_2$ Solar Cells to Preeminent and Diminished Solar Radiation
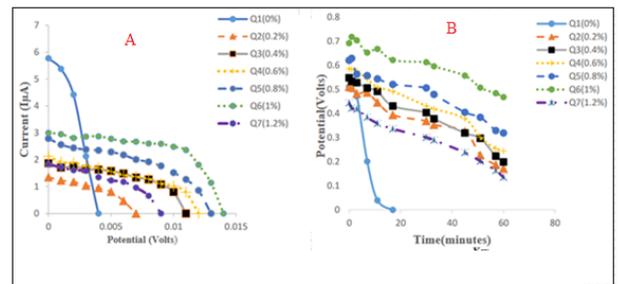
Fig. 5. Characterization of Ag-enhanced TiO$_2$ doped with allicin (A) I-V, (B) P-t

The experiments were carried in outdoor environment where the standard solar radiation energy is 1000 W/m^2 at our latitude on the earth surface [10]. The allicin doped - Ag enhanced titanium dioxide active cells were first exposed to solar

radiation in outdoor environment for 10 minutes and then then covered to block the radiation and monitored the variation of the resulting potential. The effect of potential and time upon varying the percentage composition (amount) of the luminescent material was investigated. Their resulting (I-V) and P-t characteristics are presented in the graphical representation of current (IµA) with potential (V) and potential against time of Figure 5.

The effect of varying the mass of allicin organic dopant was ensued by a distinct variation of residual potential (V) between (0.171 to 0.319) V as observed from cells Q_1 (0.2 %) through to Q_7 (1.2 %) with cell Q_6 (1 %) recording the highest (0.468 V) as observed from Figure 5 (B) in 60 minutes of the experiment. Potential surge of 0.026 V was observed from the Q_6 (1 %) profile between (0 to 1) minutes after the withdrawal of external source of optical energy. That was thought to be intensified by the extra energy from the defect relaxation of trapped charge species triggering effectuating of short wavenumber energy as the source of incident radiation was withdrawn. That regenerated suppressed energy excited higher charge carriers density from the titanium dioxide host material. The (0.049 V) residual potential disparity due to (0.8 and 1) % luminescent mass ratios was suggested to result from the proximity of the dopant optimization. [11] reported that rejuvenated optical energy significantly improved intensity due to the provision of photons by the fluorescence process. This is because the excited electrons decaying to their ground state releasing energy within the material enhancing gradual potential decay. To tune the optical energy with favourable wavelength, the target molecule ions in FSCs should be designed to enhance the excitons interaction which enhances stronger intramolecular charge transfer [12]. That enhancement twist intramolecular charge transfer state due to dopant polarity increment by a slight addition of the dopant particles. The lesser photoluminescence was attributed to the partial overlaps of the allicin stretching (σ-π) functional bonds by the alicyclics rings in the relatively (0.2 to 0.6) % dilute solvent volume ratios. [13] noted that molecules with limited aggregation-induced emission (AIE) hinder their bridging oxygens nonradioactive activation. [13] indicated that minimum FSCs potential (V) resulted because the aggregated intermolecular rotation was not fully quenched. Figure 5 (A) shows different ranges of current (I µA) and potential (V) (I-V) characteristic responses of allicin doped (Ag enhanced TiO_2) fluorescent solar cells (FSCs) with cell Q_6 (1 %) generating the highest 0.692 V and 11µA (I-V) characteristic parameters respectively in clear day light. The deviating maximum points of the I-V characteristic curves were attributed to the cells fluctuating constituent materials masses with subsequent shifting of their shunt and series resistances, along the migrating paths of charge carriers. However, further investigation showed that Q_1 (0 %) was (3 µA) short circuit current (I_{SC}) while cells Q_2 through Q_7 with (0.2 % to 1.2 %) allicin doped cells realizing (5 to 10) µA respectively. The (FF and η) of (0.618 and 4.88 %) parameters were derived from cell Q_6 (1 %). This was attributed to the enhanced optical energy interaction with the titanium dioxide habitant photo active material for eminence potential output. The improved potential

was promoted by the varied densities of relaxing charged species implied by the disparity between non-enhanced and optimally counterbalanced absorber samples [14]. To determine the optical properties of ginger plant roots, its dry powder sample was analysed using FTIR provided in Figure 5.

C. Analysis of the Effect of Gingerol Fluorescent Material Extracted from Ginger Plant Roots on Potential (V) Delay

An empirical examination of gingerol powdered material sample produced a sequence of crests presented in Figure 6.
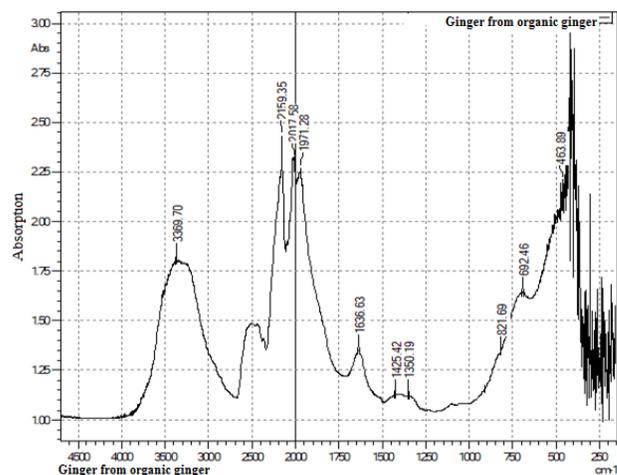
Fig. 6. FTIR absorption spectrum analysis of Gingerol luminescent material

Figure 6 shows agitation of the different functional groups in organic gingerol fluorescent material. Their pulsating moments were observed between the marginal (230 and 3850) cm^{-1} frequency bands. The conjugated bonds of (C=O), (C-OH) and (H-NH) functional groups resonating at $\tilde{V}_{(2159.35, 2017.58 \ and \ 1971.28)}$cm^{-1}, at the $\tilde{V}_{(1636.63 \ and \ 1425.42)}$cm^{-1} at $\tilde{V}_{3369.7}$ cm^{-1} wavenumbers were thought to contribute to the delayed potential due to the delay in the relaxation processes after excitation of electrons. Open-chain azo structures were thought to enhance higher photo fluorescence. That presence of distinct functional groups contributes to florescence organic materials [15]. The presence of conjugated $\sigma \ vs \ \sigma\pi$ bonds in organic materials shifted absorbed radiation to different wavelengths [16], [17]. That dominance light sensitivity by gingerol structures was derived from their low solubility aqueous solutions [18]. When illuminated with UV radiation (320 - 400 nm), the gingerol yielded yellow (565 nm) coloured radiation. [19] reported that variation of organic materials luminosity was enabled by presence of aromatic rings and carbonyl functional groups when subjected to radiation of frequencies above the visible region. That property was exploited in this study with a view to increase spectral trapped by gingerol and released later to prolong radiation to titanium dioxide photo active material.

D. Response of Gingerol Mass Doped Titanium Dioxide Solar Cells to Preeminent and Diminished Solar Radiation

The experiments were similarly carried in outdoor environment and the results obtained were as presented in

Figure 7 which shows the graphical presentations of current (IμA) with potential (V) and potential (V) against time (minutes) from the varied percentage gingerol mass of the (gingerol - Ag enhanced titanium dioxide fluorescent solar cells.
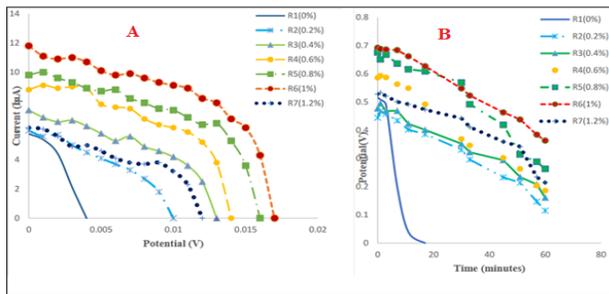
Fig. 7. Characterization of Ag-enhanced titanium dioxide doped with gingerol (A) I-V, (B) P-T

The contribution of diminished radiation was exhibited by variation of potential with time evidenced in Figure 7 (B). A sharp hyperbolic characteristic decay occurred due to extinction of visible radiation ensued by a gradual receding hyperbolic signal as displayed by profile R_5 (0.8 %) between 0 to 18 minutes. Irregular diminishing parabolic potential (V) signal of varied magnitude was observed in the rest 48 minutes due to (0.2 to 1.2) % of gingerol in the (Ag enhanced titanium dioxide host material. The (1 %) contribution of gingerol luminescent material resulted to 0.363 V delay potential after 60 minutes with the rest proportions recording below that margin. Diverging open circuit potentials (V_{OC}) generated by gingerol-doped / (Ag enhanced titanium dioxide fluorescent solar cells ranged from (0.465 - 0.692) V as observed from P-t responses. The control cell generated the lowest levels of current (μA) with negligible potential (V) sustenance of dismal time span. That evidenced that presence of luminescent material supported both charge excitation and potential delay. Excitation of electrons was to be agitated by charged species relaxing from defects of varied frequency bands. However, the I-V parameters had relatively $\{(5.77 - 11.8)$ μA increasing short current output (I_{SC}) with proportional gingerol impurity quantity increasing to (1%) limit mass ratio as depicted by Figure 7 (A). The discrepancy observed from $\{R_2$ (0.2 %) R_6 (1 %)$\}$ was attributed to the diverseness of the impurity masses. That characteristic deviation from regular hyperbolic signal was thought to emerge from the impediments of the doped material homogeneity. The highest (FF and η) of (0.294 and 5.7 %) were computed from the measured parameters of cell R_6, (1 %). [20] noted that quenching fluorescence was inhibited by the moderate compounds aggregated centres broad IR absorption. The inhomogeneity of π/δ bonds in the dopant material contributed to varied absorption frequencies [21]. That difference in levels of $(\pi - \sigma)$ bond structures resulted to radiation of varied energy levels which replaced diverging magnitudes of particles in the host/ dopant composite with distortion in varied direction [21]. The compatible acceptor and the donor particles enhanced the process of excitons dissociation with the contrary leading to lower open circuit residual potentials [22]. Similar findings by

[23] reported that ''energy donors'' should be close to the ''energy acceptor'' due to the limitation necessitated by radial energy particles inter transfer.

E. Analysis of Flourene Fluorescent Material

The resonance of flourene ionic particles after absorbing IR radiations was presented by the FTIR spectrum of Figure 8.
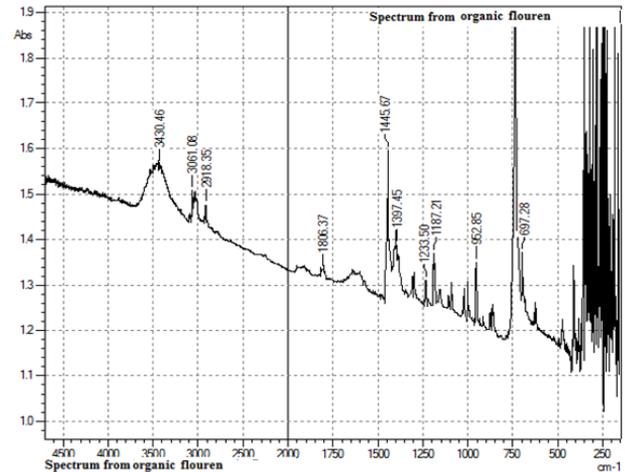
Fig. 8. FTIR absorption spectrum from flourene fluorescent organic material

The fluctuations of aromatic rings in flourene molecular structures displayed the infrared signal peaks between (230-3700) cm^{-1} wavenumbers of Figure 8. The ionic (C-N), (=C-H) and (C-H) molecular functional groups stoke shifted at (1300, 2000) cm^{-1}, $\tilde{V}_{(650, \ 697.28, \ 700)}$ cm^{-1} , $\tilde{V}_{(3043. \ 3430,3000)}$ cm^{-1} ,$\tilde{V}_{3100-3650}$ cm^{-1} and $\tilde{V}_{(500-750)}$ cm^{-1} wavenumbers. Varied atomic force and mass constants contributed to the alternating frequency bands with deviating peaks. The organic compound with the molecular formula $(C_6H_4)_2CH_2$ (diphenyl methane) appears as white powdery crystals that exhibited a characteristic, violet (380 nm) – cyan (500 nm) fluorescence when exposed to solar radiation. [24] noted that peaks in a flourene scanned spectrum originated from fluorescence of functional groups in benzene rings. The dopants can be tuned to give a particular fluorescent radiation depending on the frequency of the illuminating radiation based on its source [25]. When exposed to different monochromatic radiations, it can fluorescence giving a myriad of colours ranging from blue (450nm) to green (565 nm) and to red depending on the frequency of the illuminating radiation [2]. Similar findings by [26] indicated that flourene molecular structures with weak $\sigma\pi$ bending and stretching paired bonds emit radiations ranging from blue (450 nm) to red (650 nm) shift λ when co polymerized with other material. That property of *flourene* was exploited in this study with a view to increase spectral trapped by flourene-benzene rings and released later to prolong radiation to the photo active titanium dioxide (TiO$_2$) material. The doped material was investigated for extended time constant of energy supply by fluorescent photo cells. Their respective (I-V) and P-T characteristics are presented in the graphical representation of current (IμA) with potential (V) and potential

against time of Figure 9.
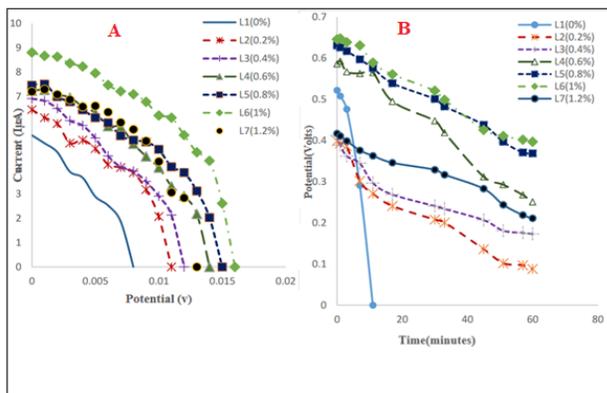
Fig. 9. Characterization of Ag-enhanced titanium dioxide doped with fluorene (A) I-V, (B) P-T

Figure 9 (B) depicts L_4 (0.6) % a signal that varies with time is (ramp) development followed by a steep potential drop in the first (0 to 3) minutes time span. A stable characteristic signal ensued for the next 8 minutes in minimum UV radiation. The cell with a relatively the least gradual decay in potential was observed to have the lowest relaxation between 20 - 45 minutes after withdrawal of the solar radiation. That signal terminated with stable characteristics of {L_2(0.2), L_3(0.4), L_5(0.8) and L_6(1)} % in the last 3 minutes of the experiment. However, outstanding 0.397 V residual potential was observed from L_6(1 %) (Flourene- Ag enhanced TiO_2) FSC after lapse of 60 minutes period. The L_4(0.6) % and L_7(1.2) % flourene FSCs exhibited unstable continuous decaying characteristics for the last 15 minutes. The low parameters generated by the rest of the cells were attributed to the dominant open – azo with low binding energies in the organic flourene impurity. The L_1 (0 %) cell low performance was indicative of internally desolate strengthened fluorescence. Majority of the radiated energy was thought to be predominated by wavenumbers between $\tilde{V}_{(650, \; 697.28, \; 700)}$ and $\tilde{V}_{(500-750)}cm^{-1}$) by $(C-H)$ ionic molecular particles at the initial stages after the withdrawal of solar radiation. With time lapse, $\tilde{V}_{(3043. \; 3430,3000)}$ cm^{-1} and $\tilde{V}_{(3100,-3650)}cm^{-1}$ molecular moments took a leading platform exhibiting the stable observed conditions by L_2(0.2 %), L_5(0.8 %) and L_6(1 %) FSCs. Figure 9 (A) shows that I-V characteristic responses in clear daylight due to charge excitation generated {(6.46 - 8.81) µA and (0.007 - 0.016) V} current and potential as observed from {L_2 (0.2 %) - L_6 (1 %)} respectively FSCs. Enhanced radiation by (1 %) flourene impurity resulted to (8.81µA and 0.648 V) short circuit (I_{SC}) and open circuit voltage (V_{OC}), with {(0.217 and 2.81 %), fill factor (FF) and power conversion efficiency (η) correspondingly. Lack of flourene in L_1 (0 %) contributed to dismal performance which was indicative of internally desolate strengthened fluorescence. The moderated frequencies were derived from fluorescence of the dopant functional groups [25]. Low recombination of charge carriers suppressed output parameters with afflicted flashes of millielectronvolts [27]. That occurred due their instantaneous radiative fluorescence in

the trapping sites. Favourable proportions were responsible for reduction of molecular ions binding energy with proportional higher rate of radiative processes [28]. The low parameters generated by the rest of the cells were attributed to the dominant open – azo with low binding energies in the organic flourene impurity. Reduced recombination of charge carriers suppressed the output parameters with afflicted flashes of millielectronvolts [29].

F. A Comparative Study of the Residual Potential (V) – Cells Doped with Different Cells

Cells that exhibited the best delay were compared using a constant mass value of the dopant and the results presented in Table 1.

Table 1
Different % organic impurities fabricated (Ag enhanced titanium dioxide) doped FSCs residual Potential (V) comparison

Cell	Q_6 (1%)	R_6 (1%)	L_6 (1%)
Residual potential (V)	0.468	0.363	0.397

A comparative influence of (allicin, gingerol and flourene) plants and synthetic origin impact on (Ag enhanced TiO_2) photo active material was presented graphically in Figure 10.
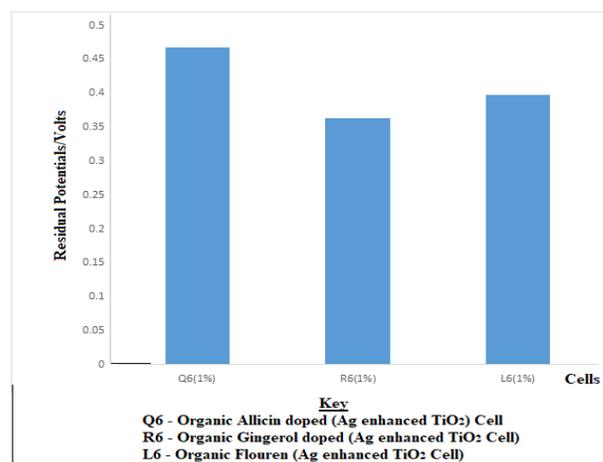
Fig. 10. Residual Potential against {(Q_6 (1 %), R_6 (1 %) and L_6 (1 %)}/(Ag enhanced titanium dioxide)}FSCs

The results of Figure 10 shows that the allicin Q_6 (1 %) ratio improved potential retention by (0.105 and 0.076) V compared to {R_6 (1 %) and L_6(1 %)} of gingerol and flouren respectively. This indicated that the (CH_2=C, C=H, H=NH, C-OH and H-NH) functional groups consolidated resonance in the secondary allicin impurity radiation delay. That improved Q_6 (1 %) performance was contributed by allicin impurity secondary material due to the suggestive longer wavenumbers energy derived from multiple functional groups. [9] indicated that the presence of σ π double bonds supported absorption for constant resonating molecular momentum. Those flexible weak $\sigma\pi$ paired bonds molecules resonated to tune the host material [30].

4. Conclusion

Energy is as an important resource to support all real-life processes. The limited spectral response of host photoactive

materials was addressed using luminescent impurities to introduce defect traps in solar irradiance dependent devices to improve their performance. The generated {(0.718, 0.692, and 0.648) V and (11, 11.8 and 8.81)} μA open circuit potential and short circuit from {allicin, gingerol and flourene}/ Ag enhanced titanium dioxide doped FSCs respectively were observed. The Fill factor (FF) and power conversion efficiency (η) derived parameters of {(0.618, 0.294 and 0.217) and (4.88, 5.7 and 2.81) % respectively resulted due to (allicin, gingerol and flourene)/ Ag enhanced titanium dioxide doped fluorescent solar cells. The IR {(290.29 – 3342.70), (463.89 – 3369.70) and (650 – 3430.46)} cm^{-2} absorption domains were observed from the (allicin, gingerol and flourene) impurities chemical characterization using a Shimadzu FTIR 2014 spectrometer. The presence of varied multiple resonating open azo structures resulted to delayed potentials. The impressive sustained (0.468, 0.363 and 0.397) V potentials after 60 minutes due to the many conjugated pi bonds as confirmed by FT IR analysis absorption by unpaired and intertwined multiple bonds of the photo luminescent material. The different organic fluorescent materials in this study prolonged the duration of solar cell output potential. The results obtained show that doping of titanium dioxide with fluorescent materials had promising properties for potential application for improved efficiency of fluorescent solar cells.

References

[1] Tsai SR, Hamblin MR. Biological effects and medical applications of infrared radiation. Journal of Photochemistry and Photobiology B: Biology. 2017; 170:197–207.

[2] Herrmann A, Völksch G, Ehrt D. Tb^{3+} as probe ion—Clustering and phase separation in borate and borosilicate glasses. International Journal of Applied Glass Science. 2019;10(4):532–45.

[3] McArthur EA, Morris-Cohen AJ, Knowles KE, Weiss EA. Charge carrier resolved relaxation of the first excitonic state in CdSe quantum dots probed with near-infrared transient absorption spectroscopy. The Journal of Physical Chemistry B. 2010;114(45):14514–20.

[4] Li W, Long R, Tang J, Prezhdo OV. Influence of defects on excited-state dynamics in lead halide perovskites: time-domain ab initio studies. The journal of physical chemistry letters. 2019;10(13):3788–804.

[5] Chen S, Du J, Shen L, Chen W. In situ decoration of Ag nanoparticles on hierarchical TiO$_2$ nanowire nanofibers with enhanced catalytic activity used for the removal of 4-nitrophenol. Journal of Physics and Chemistry of Solids. 2021; 149:109784.

[6] Ruggenthaler M, Tancogne-Dejean N, Flick J, Appel H, Rubio A. From a quantum-electrodynamical light–matter description to novel spectroscopies. Nature Reviews Chemistry. 2018;2(3):1–16.

[7] Lee SH, Jeon HB, Hwang GH, Kwon YS, Lee JS, Park GT, et al. Effects of poly (ethylene-co-glycidyl methacrylate) on the microstructure, thermal, rheological, and mechanical properties of thermotropic liquid crystalline polyester blends. Polymers. 2020;12(9):2124.

[8] Guo MX, Yang L, Jiang ZW, Peng ZW, Li YF. Al-based metal-organic gels for selective fluorescence recognition of hydroxyl nitro aromatic compounds. Spectrochimica Acta Part A: Molecular and Biomolecular Spectroscopy. 2017; 187:43–8.

[9] Spence C. On the changing colour of food & drink. International Journal of Gastronomy and Food Science. 2019 Oct 1; 17:100161.

[10] Brun P, Zimmermann NE, Hari C, Pellissier L, Karger DN. Global climate-related predictors at kilometre resolution for the past and future. Earth System Science Data Discussions. 2022; 2022:1–44.

[11] Román Castellanos L, Hess O, Lischner J. Dielectric engineering of hot-carrier generation by quantized plasmons in embedded silver nanoparticles. The Journal of Physical Chemistry C. 2021;125(5):3081–7.

[12] Xue J, Liang Q, Zhang Y, Zhang R, Duan L, Qiao J. High-efficiency near-infrared fluorescent organic light-emitting diodes with small efficiency roll-off: a combined design from emitters to devices. Advanced Functional Materials. 2017;27(45):1703283.

[13] Zhai X, Chen R, Shen W. Aggregation-induced emission active luminescent polymeric nanofibers: From design, synthesis, fluorescent mechanism to applications. TrAC Trends in Analytical Chemistry. 2022; 146:116502.

[14] Soares Lins E. Dual Optical Frequency Comb Time-resolved Spectroscopy for Surface-Enhanced Spectro electro chemistry [PhD Thesis]. University of Saskatchewan; 2022.

[15] Zhang FL, Zhou BW, Yan ZZ, Zhao J, Zhao BC, Liu WF, et al. 6-Gingerol attenuates macrophages pyroptosis via the inhibition of MAPK signaling pathways and predicts a good prognosis in sepsis. Cytokine. 2020; 125:154854.

[16] Abderrazak Y, Bhattacharyya A, Reiser O. Visible-Light-Induced Homolysis of Earth-Abundant Metal-Substrate Complexes: A Complementary Activation Strategy in Photoredox Catalysis. Angewandte Chemie International Edition. 2021;60(39):21100–15.

[17] Alexey K, Jan G, Nino L, David F, Juri Z, Svetlana S. Light-Induced Reversible Change of Roughness and Thickness of Photosensitive Polymer Brushes. 2016;

[18] Mulia K, Risqi UY, Pane IF, Krisanti EA. Formulation, characterization, and release property of antioxidant supplement capsule with red ginger oleoresin extract-loaded chitosan microparticles. In: Journal of Physics: Conference Series. IOP Publishing; 2019. p. 062008.

[19] Lee HJ, Shim JW, Lee JJ, Lee WJ. The Encapsulation of Natural Organic Dyes on TiO$_2$ for Photochromism Control. International Journal of Molecular Sciences. 2023;24(9):7860.

[20] Zhao L, Liu Y, Xing R, Yan X. Supramolecular Photothermal Effects: A Promising Mechanism for Efficient Thermal Conversion. Angewandte Chemie. 2020;132(10):3821–9.

[21] Wang Z, Liu Y, Wang B. Bond-Orbital-Resolved Piezoelectricity in Sp2-Hybridized Monolayer Semiconductors. Materials. 2022;15(21):7788.

[22] Zhang Z, Li L, Xu C, Jin P, Huang M, Li Y, et al. Single photovoltaic material solar cells with enhanced exciton dissociation and extended electron diffusion. Cell Reports Physical Science. 2022;3(6):100895.

[23] Herrmann A, Tsekrekas E, Möncke D, Clare AG. Luminescence-site symmetry correlations in Dy^{3+} doped alkali-alkaline earth orthoborates of the type XZBO$_3$ with X= Li, Na, K and Z= Mg, Ca, Ba. Journal of Luminescence. 2022; 241:118429.

[24] Mohamed MG, Hu HY, Madhu M, Samy MM, Mekhemer IM, Tseng WL, et al. Ultrastable two-dimensional fluorescent conjugated microporous polymers containing pyrene and fluorene units for metal ion sensing and energy storage. European Polymer Journal. 2023; 189:111980.

[25] Xie LH, Yang SH, Lin JY, Yi MD, Huang W. Fluorene-based macromolecular nanostructures and nanomaterials for organic (opto) electronics. Philosophical Transactions of the Royal Society A: Mathematical, Physical and Engineering Sciences. 2013; 371(2000): 20120337.

[26] Peterson KA. Electronic Structure, Chemical Mechanism, and Morphology in Doping Organic Semiconductors.

[27] Strunk J. Heterogeneous Photocatalysis: From Fundamentals to Applications in Energy Conversion and Depollution. John Wiley & Sons; 2021.

[28] Al-Alwani MA, Mohamad AB, Ludin NA, Kadhum AAH, Sopian K. Dye-sensitised solar cells: Development, structure, operation principles, electron kinetics, characterisation, synthesis materials and natural photo sensitisers. Renewable and Sustainable Energy Reviews. 2016; 65:183–213.

[29] Chen S, Fu Y, Ishaq M, Li C, Ren D, Su Z, et al. Carrier recombination suppression and transport enhancement enable high-performance self-powered broadband Sb2Se3 photodetectors. InfoMat. 2023; e12400.

[30] Kim JH, Ahmad Z, Kim Y, Kim W, Ahn H, Lee JS, et al. Decoupling critical parameters in large-range crystallinity-controlled polypyrrole-based high-performance organic electrochemical transistors. Chemistry of Materials. 2020;32(19):8606–18.